J. Fluid Mech. (1980), *vol.* 99, *part* 2, *pp.* 321–342
Printed in Great Britain

Boundary-layer velocities and mass transport in short-crested waves

By J. R. C. HSU, R. SILVESTER AND Y. TSUCHIYA†

Department of Civil Engineering, The University of Western Australia, Nedlands, Western Australia

(Received 12 July 1978 and in revised form 26 November 1979)

A comprehensive programme of research is being undertaken on short-crested waves produced by obliquely reflecting waves from a rigid vertical wall. This has included a new wave theory to third-order approximation. The second-order Eulerian water-particle velocities throughout the bottom boundary layer are now investigated. From this the resulting mass transport is considered to the first approximation. The vertical velocity component has a non-zero value within and just beyond the boundary layer. The limiting two-dimensional cases of progressive and standing waves are obtained and compared with published results. Comparison is also made with available experimental data. Graphs of some analytical solutions are presented.

1. Introduction

Progressive and standing waves have been examined for oscillatory motions, as well as net movements of water particles known as mass transport. Theoretical solutions and experimental verification have been provided for inviscid conditions for the interior of the fluid and for the viscous bottom boundary layer, the latter for both laminar and turbulent theory.

The case for short-crested waves has received very little attention. This is unfortunate since it is submitted that such systems are more predominant in nature than the progressive and standing waves normally analysed theoretically and tested experimentally in the flume. Short-crested waves arise from oblique reflexion on vertical or sloping surfaces, diffraction from either end of an island structure, differential refraction across the continental shelf, swell arriving from two storm centres simultaneously, and waves within or just outside a fetch. However, only a special case of two interacting wave trains of equal amplitude and period is considered in this work.

Short-crested waves can be equated to two progressive waves of the same amplitude propagating at an angle to each other. The resultant water-particle motions vary spatially both in the vertical and horizontal directions. The simple case of two wave trains of equal height and period is shown schematically in figure 1, where it is seen that rectilinear and elliptical orbits exist along certain alignments. Along that of the combined crest propagation (i.e. at $y/L_y = \frac{1}{2}, 1, \ldots$) water-particle orbits are in a vertical plane. Half-way between, rectilinear horizontal oscillations occur (i.e. at $y/L_y = \frac{1}{4}, \frac{3}{4}, \ldots$); where $y/L_y = \frac{1}{8}, \frac{3}{8}, \frac{5}{8}, \ldots$, the orbits are ellipses at an angle to the vertical which depends upon their depth, being in a horizontal plane at the bed.

† Permanent address: Disaster Prevention Research Institute, Kyoto University, Japan.

0022-1120/80/4485-1500 $02.00

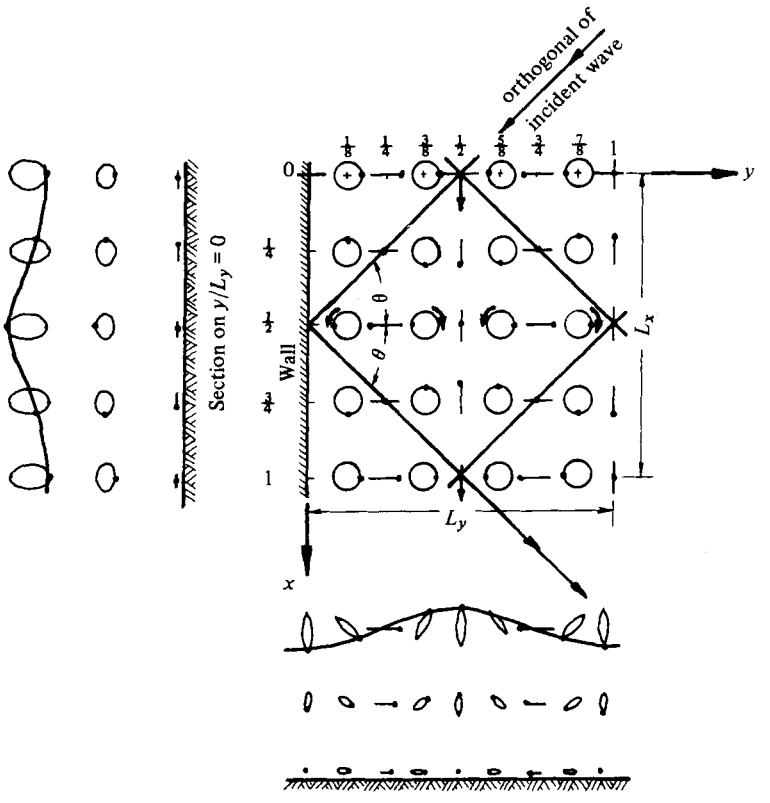

FIGURE 1. Definition sketch of short-crested wave produced by reflexion showing co-ordinates and ideal orbital motions at various depths. $\theta = 45°$.

The maximum orbital velocities, resulting from the combined wave height, are nearly double those of the progressive waves making up the system. The elliptical orbits between the $\frac{1}{4}L_y$ and $\frac{1}{2}L_y$ etc. alignments extend right to the bed. It is easy to see that these motions will aid the suspension of bed material. Silvester (1972) has described sand-ripple formations on a sandy bed produced by waves reflected obliquely from a vertical wall. He has also stressed the importance of wave reflexion in coastal sediment transport (Silvester 1977).

Hsu, Tsuchiya & Silvester (1979) have derived a third-order approximation for particle motions in short-crested waves by a perturbation method. This yields the two limiting conditions of Stokes and standing waves. The results at the bed from this wave theory will be used as the matching condition to derive motions within the bottom layer.

Time-varying water-particle velocities within the boundary layer are important in understanding peak orbital velocities very close to the bed, where sedimentary particles can be influenced. The changing orientations of horizontal components across the crest length, which can constitute elliptical patterns of motion, provide additional lifting capacity. The vertical velocity component generated within the boundary layer for small fractions of the wave cycle could help sustain particles in suspension for longer periods. This vertical component has been alluded to by Stuart

(1963), Schlichting (1968), Noda (1968, 1970), Isaacson (1976) and Liu & Davis (1977), for the two-dimensional cases, where a secular term appeared in their solutions. This will be further discussed in § 3.

Using a superposition of linear velocity potentials and a Lagrangian formulation, Mei, Liu & Carter (1972) derived a first approximation to the mass-transport velocity within the bottom boundary layer. Their final expression for the velocity component along the wall cannot be reduced to the limiting progressive wave as given by Longuet-Higgins (1953). Similar analyses by Hunt & Johns (1963), Tanaka, Irie & Ozasa (1972) and Dore (1974) all refer to the outer edge of the bottom layer. Hence, it is believed that the Eulerian water-particle motions to second order and the vertical component of mass transport, herein presented for short-crested waves, have not been derived previously.

Experiments by Tanaka *et al.* (1972) utilized coal and sand tracers in a wave flume 2·5 m wide, but only directions were reported, not rate of transport. No quantitative measurements have been reported on the kinematics or mass transport in short-crested waves within the bottom layer until Hsu (1977) reported the use of polystyrene beads smaller in diameter than the boundary layer and with slight negative buoyancy. Their motions at the bed over the full region of the short-crested system were observable through the transparent ceiling of a tunnel beneath a wave basin. Cine photography of these tracers permitted spot positioning every $\frac{1}{24}$ second, but every second frame was used to compute the velocities and mass transport over several wave cycles. A comparison is made with the new theory.

The limiting two-dimensional cases are also derived for both the Eulerian water-particle velocities and mass transport. The latter agree with solutions by Longuet-Higgins (1953) for progressive and standing waves.

2. Third-order approximation to short-crested waves

Hsu *et al.* (1979) have derived a third-order approximation of wave theory by a perturbation method. To solve the basic governing equations for describing the three-dimensional irrotational, inviscid wave motion, all variables were non-dimensionalized. Let ϵ be the small parameter ka, in which a is the wave amplitude of the short-crested waves to the first-order approximation, then the following dimensionless quantities ($\hat{}$) may be introduced:

$$\left.\begin{aligned} &\hat{\phi}(\hat{x}, \hat{y}, \hat{z}, \hat{t}) = k^2\epsilon^{-1}(gk)^{-\frac{1}{2}}\phi(x, y, z, t), \\ &\hat{x} = kx, \quad \hat{y} = ky, \quad \hat{z} = kz, \quad \hat{t} = \sigma t, \quad \hat{d} = kd, \\ &\omega = \sigma/(gk)^{\frac{1}{2}}, \end{aligned}\right\} \tag{1}$$

in which σ is the angular frequency of incident and reflected waves or $2\pi/T$ (T being the wave period), k is the wavenumber or $2\pi/L$ (L being the wavelength of the component waves), x, y and z are the Cartesian co-ordinates, t the time, g the acceleration due to gravity and ϕ the wave velocity potential. Let L_x and L_y be the horizontal distances between crests in the x and y directions respectively. Then the components of the wavenumber k may be defined respectively as

$$m_1 = 2\pi/L_x = k\sin\theta = mk, \quad n_1 = 2\pi/L_y = k\cos\theta = nk, \tag{2}$$

in which θ is the incident angle of the wave orthogonal measured from the normal to the wall (see figure 1). When the incident angle vanishes, a normal standing wave appears, whilst a progressive wave results when $\theta = \frac{1}{2}\pi$. From equation (2),

$$m_1^2 + n_1^2 = k^2, \quad m^2 + n^2 = 1. \tag{3}$$

The perturbed solutions are assumed to be

$$\left.\begin{aligned} \hat{\phi} &= \hat{\phi}_0 + \epsilon\hat{\phi}_1 + \tfrac{1}{2}\epsilon^2\hat{\phi}_2 + O(\epsilon^3), \\ \omega &= \omega_0 + \epsilon\omega_1 + \tfrac{1}{2}\epsilon^2\omega_2 + O(\epsilon^3). \end{aligned}\right\} \tag{4}$$

The carets denoting dimensionless quantities in this section will now be omitted for simplicity, unless otherwise specified. Only the final expressions for ϕ and ω in each order of approximation are listed below.

First-order approximation (at order ϵ^0),

$$\phi_0 = \omega_0 \frac{\cosh(z+d)}{\sinh d} \cos ny \sin(mx - t), \quad \omega_0 = [\tanh d]^{\frac{1}{2}}. \tag{5}$$

Second-order approximation (at order ϵ),

$$\left.\begin{aligned} \phi_1 &= \beta_1 t + \beta_2 \cosh 2(z+d) \cos 2ny \sin 2(mx - t) + \beta_3 \cosh 2m(z+d) \sin 2(mx - t), \\ \omega_1 &= 0, \end{aligned}\right\} \tag{6}$$

in which

$$\left.\begin{aligned} \beta_1 &= \tfrac{1}{8}(-\omega_0^{-3} + \omega_0), \\ \beta_2 &= \frac{3}{16}\frac{(\omega_0^{-7} - \omega_0)}{\cosh 2d}, \quad \beta_3 = \frac{(1+\omega_m^4)K_1}{16\cosh 2md}. \end{aligned}\right\} \tag{7}$$

Here

$$\left.\begin{aligned} K_1 &= \frac{[(4m^2-1)\omega_0^{-3} - 3\omega_0]}{[(1+\omega_m^4) - m(\omega_m/\omega_0)^2]}, \\ K_2 &= (1+\omega_m^4)K_1, \quad \omega_m = [\tanh(md)]^{\frac{1}{2}}. \end{aligned}\right\} \tag{8}$$

The third-order approximation (at order ϵ^2) was presented by Hsu *et al.* (1979) but is not required in the following analysis.

3. Laminar boundary at the bottom

A perturbation method is used to derive an approximate solution to the three-dimensional viscous laminar boundary-layer equations on a rigid and smooth horizontal bed for this short-crested wave system. The newly developed wave theory (Hsu *et al.* 1979) is used to specify the Eulerian velocities at the outer edge of the boundary layer. The Eulerian water-particle velocity field within the bottom layer is then obtained by solving the dimensionless governing equations to satisfy the various boundary conditions. Effects of wave damping due to viscosity are neglected. Only small-amplitude motions are considered.

Approximate solution to laminar boundary layer

Taking rectangular Cartesian co-ordinates (x, y, z) with associated components of fluid velocity (u, v, w) in each direction respectively, it is assumed that *the z axis is vertically upwards from the bed* and the x and y axes horizontal (x along the reflecting wall and y normal to it).

In the motion of a viscous medium over a fixed plate, the velocities (u, v) increase more or less rapidly from zero at bed to the values of (U, V) given by potential theory in an ideal fluid. Prandtl (1904) recognized that for small viscosity this domain of increasing velocity extended in practice only to a relatively small distance from the bed.

Since the thickness of the bottom layer is small compared with the characteristic length scales of the wave train, the Prandtl boundary layer equations are applicable to the motion within it. Introducing the subscripts x, y, z and t as the partial derivatives to the physical quantities, the governing Navier–Stokes equations in dimensional form are

$$u_t + uu_x + vu_y + wu_z = -p_x/\rho + \nu(u_{zz} + u_{xx} + u_{yy}), \tag{9}$$

$$v_t + uv_x + vv_y + wv_z = -p_y/\rho + \nu(v_{zz} + v_{xx} + v_{xy}), \tag{10}$$

where ρ is the density of fluid, p is the wave pressure and ν the kinematic viscosity. It is reasonable to assume that $u_{zz} \gg u_{xx}$ or u_{yy}, and so on, after examining the orders of magnitude of various terms. The continuity equation is given as

$$u_x + v_y + w_z = 0, \tag{11}$$

and the pressure equations at the outer edge of the boundary layer are

$$-p_x/\rho = U_t + UU_x + VU_y, \tag{12}$$

$$-p_y/\rho = V_t + UV_x + VV_y, \tag{13}$$

for the x and y components respectively, subject to the boundary conditions $u = v = w = 0$ at $z = 0$, and $u = U$ and $v = V$ as $z \to \infty$, where U and V are the Eulerian particle velocity components at the outer edge of the boundary layer, obtained from the wave motion in the interior of the fluid.

Introducing the dimensionless quantities,

$$\left.\begin{aligned} &\hat{x} = kx, \quad \hat{y} = ky, \quad \hat{z} = [(gk)^{\frac{1}{2}}/\nu]^{\frac{1}{2}} z, \quad \hat{d} = kd, \quad \hat{t} = \sigma t, \\ &\hat{\phi}(\hat{x}, \hat{y}, \hat{z}, \hat{t}) = k^2 \epsilon^{-1} (gk)^{-\frac{1}{2}} \phi(x, y, z, t), \\ &\hat{u} = (k/g)^{\frac{1}{2}} u, \quad \hat{v} = (k/g)^{\frac{1}{2}} v, \quad \hat{w} = [\nu(gk)^{\frac{1}{2}}]^{-\frac{1}{2}} w, \\ &\omega = \sigma/(gk)^{\frac{1}{2}}, \quad \hat{p} = (k/\rho g) p, \end{aligned}\right\} \tag{14}$$

into (9)–(13), the governing equations can be transformed into dimensionless form (omitting the carets):

$$\omega u_t + uu_x + vu_y + wu_z = \omega U_t + UU_x + VU_y + u_{zz}, \tag{15}$$

$$\omega v_t + uv_x + vv_y + wv_z = \omega V_t + UV_x + VV_y + v_{zz}, \tag{16}$$

and

$$u_x + v_y + w_z = 0. \tag{17}$$

An additional change of variable for z within the boundary layer is also introduced (Noda 1970),

$$\zeta = (\tfrac{1}{2}\omega_0)^{\frac{1}{2}} z, \tag{18}$$

or physically $\zeta = z/(\nu T/\pi)^{\frac{1}{2}}$ in dimensional form, as a measure of distance from the bed within the boundary layer. It is worth noting that $\zeta = 2\pi$ corresponds to the outer edge of the boundary layer, as the boundary-layer thickness is usually calculated by $\delta = 2(\pi\nu T)^{\frac{1}{2}}$ (i.e. from replacing z in the dimensional form of equation (18) by the value of δ).

To ease the repeated listings for the dimensionless velocity components (U, V, W) and (u, v, w), assume the expansion series in a small parameter ϵ in the abstract form,

$$f = \sum_{j=1}^{\infty} \epsilon^j f_j \quad \text{for} \quad (U, V, W) \tag{19}$$

and

$$f = \sum_{j=1}^{\infty} \epsilon^j f_j = \sum_{j=1}^{\infty} \epsilon^j (f_{jp} + f_{js}) \quad \text{for} \quad (u, v, w). \tag{20}$$

In (20), all f_{jp} are time-dependent and f_{js} time-independent terms.

For the water-particle velocity components in dimensionless form, Hsu *et al.* (1979) have shown from the introduced variable transformations that the following conditions exist:

$$u = \epsilon\phi_x, \quad v = \epsilon\phi_y, \quad w = \epsilon\phi_z, \tag{21}$$

in which ϕ is the perturbed value of (4) by inserting the solutions of ϕ_0 and ϕ_1 from (5) and (6).

Let the Eulerian particle velocity at the outer edge of the boundary layer be represented by the velocity on the bed from the inviscid wave theory for $z = -d$. The dimensionless quantities (U, V, W) are therefore

$$\begin{aligned} U = \epsilon\phi_x|_{z=-d} &= \epsilon(m\omega_0/\sinh d)\cos ny\cos(mx-t) + \epsilon^2(2m\beta_2\cos 2ny\cos 2(mx-t) \\ &\qquad + 2m\beta_3\cos 2(mx-t)] \\ &= \epsilon U_1 + \epsilon^2 U_2 + O(\epsilon^3), \end{aligned} \tag{22}$$

and

$$\begin{aligned} V = \epsilon\phi_y|_{z=-d} &= -\epsilon(n\omega_0/\sinh d)\sin ny\sin(mx-t) - \epsilon^2[2n\beta_2\sin 2ny\sin 2(mx-t)] \\ &= \epsilon V_1 + \epsilon^2 V_2 + O(\epsilon^3), \end{aligned} \tag{23}$$

but

$$W = \epsilon\phi_z|_{z=-d} = 0, \quad \text{more particularly at the bed.} \tag{24}$$

Inserting the perturbed quantities of velocities from (20) and (22)–(24) into (15)–(17), and collecting terms of each order in ϵ yields the necessary equations to each order of approximation. To first order in ϵ, the governing equations in dimensionless form are

$$u_{1t} - \tfrac{1}{2}u_{1\zeta\zeta} = U_{1t}, \tag{25a}$$

$$v_{1t} - \tfrac{1}{2}v_{1\zeta\zeta} = V_{1t}, \tag{25b}$$

$$u_{1x} + v_{1y} + (\tfrac{1}{2}\omega_0)^{\frac{1}{2}} w_{1\zeta} = 0, \tag{25c}$$

with the boundary conditions

$$u_1 = v_1 = w_1 = 0 \quad \text{at} \quad \zeta = 0, \tag{26}$$

and the matching conditions

$$u_{1p} = U_1, \quad v_{1p} = V_1 \quad \text{at} \quad \zeta \to \infty. \tag{27}$$

The solutions of (25) that satisfy the boundary conditions of (26) and (27) are given in dimensionless form as

$$u_1 = \frac{m\omega_0}{\sinh d}\cos ny\,[\cos(mx-t) - e^{-\zeta}\cos(mx-t+\zeta)], \tag{28}$$

$$v_1 = -\frac{n\omega_0}{\sinh d}\sin ny\,[\sin(mx-t) - e^{-\zeta}\sin(mx-t+\zeta)], \tag{29}$$

$$w_1 = \frac{\omega_0^{\frac{1}{2}}}{\sinh d}\cos ny\,[2^{\frac{1}{2}}\zeta\sin(mx-t) - \sin(mx-t+\tfrac{1}{4}\pi) + e^{-\zeta}\sin(mx-t+\zeta+\tfrac{1}{4}\pi)]. \tag{30}$$

The physical meaning of the terms in (30) is that outside the bottom boundary layer the third term tends to zero, whilst the second term represents the displacement effect of the boundary layer on the external flow, or, in other words, the diffusion of periodic vorticity (Stuart 1963). The so-called 'secular term', that is the first term in the bracket of (30), fulfils the need of the continuity condition (25*c*). Its presence is entirely consistent with unsteady boundary-layer theory where an external mean flow exists.

The limiting two-dimensional expressions for either progressive waves (with $m = 1$ and $n = 0$) or normal standing waves (with $m = 0$ and $n = 1$) are readily obtainable. The results so reduced are similar to those from Stuart (1963), Schlichting (1968), Noda (1968, 1970), Isaacson (1976) and Liu & Davis (1977), for the two-dimensional cases, in which the secular term in ζ also appears in the w_1 derivation.

The secular term ζ for w_1 of (30) becomes infinite theoretically at the outer edge of the boundary layer, because this layer is considered of infinite thickness analytically. Since in practice it is of finite size, in fact only some millimetres in magnitude, it is deemed reasonable to use the value of ζ at the edge of the boundary layer which has been shown from numerical evaluation to approximate 2π (see explanation immediately after equation (18)). This is the dimensional meaning of (18), and therefore represents the condition at the outer edge of the bottom layer. An alternative value to 2π might be assumed where the horizontal velocities are, say, within 1 % of the free-stream values.

From a theoretical point of view, the boundary layer being considered to be of infinite extent in the z direction, it is necessary to conclude that the transition of (u, v) into (U, V) is asymptotic in nature. However, equations (28) and (29) show precisely that these free-stream velocities (U, V) are reached very rapidly, and the assumption of a finite boundary-layer thickness is therefore justified and meaningful.

To the second order, the dimensionless governing equations are given by

$$u_{2t} - \tfrac{1}{2}u_{2\zeta\zeta} = U_{2t} + \omega_0^{-1}(U_1 U_{1x} + U_1 U_{1y} - \omega_0^{-1}(u_1 u_{1x} + v_1 u_{1y} + (\tfrac{1}{2}\omega_0)^{\frac{1}{2}} w_1 u_{1\zeta}), \tag{31}$$

$$v_{2t} - \tfrac{1}{2}v_{2\zeta\zeta} = V_{2t} + \omega_0^{-1}(U_1 V_{1x} + V_1 V_{1y}) - \omega_0^{-1}(u_1 v_{1x} + v_1 v_{1y} + (\tfrac{1}{2}\omega_0)^{\frac{1}{2}} w_1 v_{1\zeta}), \tag{32}$$

$$u_{2x} + v_{2y} + (\tfrac{1}{2}\omega_0)^{\frac{1}{2}} w_{2\zeta} = 0. \tag{33}$$

To determine the current unknowns u_2 and v_2, the given solutions of u_1, v_1 and w_1 from equations (28)–(30) and U_1, U_2, V_1 and V_2 from (22) and (23) are substituted into (31) and (32). The resulting partial differential equations contain both time-dependent and time-independent terms. These are represented as p and s respectively in the subscripts, where p stands for periodic and s for steady-state (i.e. time-independent). Hence, using the method of Schlichting (1968) (Iwagaki & Tsuchiya 1966), the complete solution of u_2 and v_2 can be found. Accordingly, it is assumed that the superposition holds,

$$u_2 = u_{2p} + u_{2s}, \quad v_2 = v_{2p} + v_{2s}, \tag{34}$$

subject to the boundary conditions

$$\left.\begin{aligned} &u_{2p} = u_{2s} = 0 \quad \text{at} \quad \zeta = 0, \\ &u_{2p} = U_2 \quad \text{and} \quad \partial u_{2s}/\partial z = 0 \quad \text{at} \quad \zeta \to \infty, \end{aligned}\right\} \tag{35}$$

and

$$\left.\begin{aligned} &v_{2p} = v_{2s} = 0 \quad \text{at} \quad \zeta = 0, \\ &v_{2p} = V_2 \quad \text{and} \quad \partial v_{2s}/\partial z = 0 \quad \text{at} \quad \zeta \to \infty. \end{aligned}\right\} \tag{36}$$

The complete solutions of (31) and (32) are finally given in dimensionless form as

$$u_2 = Q_1\cos 2X + (6Q_3 - 4Q_2)e^{-\zeta}\cos(2X+\zeta) + (Q_3 - Q_2)e^{-2\zeta}\cos 2(X+\zeta) - 2\sqrt{2}\,Q_3\zeta e^{-\zeta}\cos(2X+\zeta-\tfrac{1}{4}\pi) - (Q_1 - 5Q_2 + 7Q_3)e^{-\sqrt{(2)}\zeta}\cos(2X+\sqrt{2}\,\zeta) + Q_3[2e^{-\zeta}(\sin\zeta - 2\cos\zeta) - 2\sqrt{2}\,\zeta e^{-\zeta}\cos(\zeta-\tfrac{1}{4}\pi) + e^{-2\zeta} + 3], \tag{37}$$

and

$$v_2 = [-Q_4\sin 2X - 2Q_5 e^{-\zeta}\sin(2X+\zeta) + 2\sqrt{2}\,Q_5\zeta e^{-\zeta}\sin(2X+\zeta-\tfrac{1}{4}\pi) + (Q_4+2Q_5)e^{-\sqrt{(2)}\zeta}\sin(2X+\sqrt{2}\,\zeta)]\sin 2ny + Q_5[2n^2(4e^{-\zeta}\sin\zeta + e^{-2\zeta} - 1) + 2\sqrt{2}\,\zeta e^{-\zeta}\sin(\zeta-\tfrac{1}{4}\pi) + 2e^{-\zeta}\cos\zeta - e^{2\zeta} - 1]\sin 2ny, \tag{38}$$

in which $X = (mx - t)$

and

$$\left.\begin{aligned} Q_1 &= 2m\beta_2\cos 2ny + 2m\beta_3,\\ Q_2 &= \frac{m\omega_0}{8\sinh^2 d}[\cos 2ny + 2m^2 - 1],\\ Q_3 &= \frac{m\omega_0}{8\sinh^2 d}[\cos 2ny + 1], \end{aligned}\right\} \tag{39}$$

$$\left.\begin{aligned} Q_4 &= 2n\beta_2,\\ Q_5 &= n\omega_0/(8\sinh^2 d). \end{aligned}\right\} \tag{40}$$

Then w_2 is obtained from the continuity equation of (33), with the boundary condition that $w_2 = 0$ at $\zeta = 0$, and is given as

$$w_2 = (2/\omega_0)^{\frac{1}{2}}[Q_6\zeta\sin 2X - Q_7\sin(2X+\tfrac{1}{4}\pi) - 8Q_8 e^{-\zeta}\sin(2X+\zeta+\tfrac{1}{4}\pi) - Q_8 e^{-2\zeta}\sin(2X+2\zeta+\tfrac{1}{4}\pi) + Q_9\zeta e^{-\zeta}\sin(2X+\zeta) + Q_{10}e^{-\sqrt{(2)}\zeta}\sin(2X+\sqrt{2}\,\zeta+\tfrac{1}{4}\pi)] + (2/\omega_0)^{\frac{1}{2}}\{2n^3Q_5\cos 2ny[4\sqrt{2}\,e^{-\zeta}\sin(\zeta+\tfrac{1}{4}\pi) + e^{-2\zeta} + 2\zeta - 5] + 2nQ_5\cos 2ny[2\zeta e^{-\zeta}\sin\zeta + 2e^{-\zeta}\cos\zeta - \tfrac{1}{2}e^{-2\zeta} + \zeta - \tfrac{3}{2}]\}, \tag{41}$$

in which

$$\left.\begin{aligned} Q_6 &= 2mQ_1 + 2nQ_4\cos 2ny,\\ Q_7 &= m[Q_1 - 5Q_2 + 7Q_3 + 9(Q_2 - Q_3)/\sqrt{2}] + n[Q_4 + 2Q_5]\cos 2ny,\\ Q_8 &= m(Q_3 - Q_2)/\sqrt{2},\\ Q_9 &= 4mQ_3 + 4nQ_5\cos 2ny,\\ Q_{10} &= m(Q_1 - 5Q_2 + 7Q_3) + n(Q_4 + 2Q_5)\cos 2ny. \end{aligned}\right\} \tag{42}$$

It is clearly seen from (37), (38) and (41) that u_2, v_2 and w_2 consist of periodic parts with and without boundary-layer variables, plus the time-independent terms which are varying across the direction normal to the wall. However, there are secular terms, deriving from w_1 of (30).

The time-independent parts of these second-order velocities for just beyond the bottom layer, at $\zeta \to \infty$ for the horizontal components, and at $\zeta = 2\pi$ for the vertical velocity, are given as

$$\left.\begin{aligned} u'_{2s} &= \frac{3m\omega_0}{8\sinh^2 d}(\cos 2ny + 1),\\ v'_{2s} &= -\frac{n\omega_0}{8\sinh^2 d}(2n^2 + 1)\cos 2ny,\\ w'_{2s} &= \frac{n^2\omega_0^{\frac{1}{2}}}{8\sinh^2 d}(21{\cdot}4n^2 + 13{\cdot}5)\cos 2ny. \end{aligned}\right\} \tag{43}$$

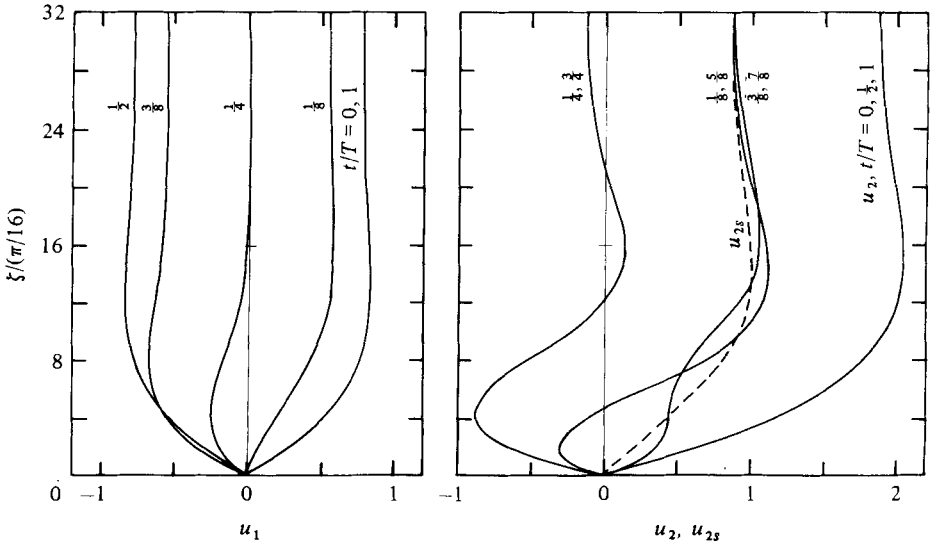

FIGURE 2. Profiles of Eulerian water-particle velocities u_1, u_2 and u_{2s} through the bottom boundary layer at various time steps. $\theta = 45°$, $d/L = 0{\cdot}1$, $y/L_y = 0$ and 1.

Equations for u'_{2s} and v'_{2s} in (43) agree with conclusions reached by Dore (1974), but in the present study w'_{2s} is not zero as would be obtained by inserting $a_+ = a_- = a$ and replacing m by n in Dore's paper. This finite value of w'_{2s} is acceptable in the short-crested wave system, since the time-averaged particle paths are three-dimensional in nature when viscosity is taken into account, as noted by Dore (1973) and private communication (1978), and the boundary condition for w_1 in (24) at the edge of the boundary layer is imposed. The value of w'_{2s} can be readily traced back from the continuity equations (33) and the time-independent parts in v_2 of (38) for satisfying the condition $w_2 = 0$ at $\zeta = 0$. In the two-dimensional case of the progressive wave, w'_{2s} vanishes since $n = 0$, but it has a finite value in normal standing waves.

Examples of the maximum Eulerian water-particle velocity profiles through the bottom boundary layer are graphed in figures 2 and 3, as functions of the relative time step (t/T), for the case of relative water depth $d/L = 0{\cdot}1$ and incident angle $\theta = 45°$. Here the reading of the vertical scale at 32 is for $\zeta = 2\pi$, representing the condition at the outer edge of the bottom layer, as discussed previously. The curve u_2 from (37) being the sum of the time-dependent parts u_{2p} and the time-independent terms u_{2s}, exhibits strong asymmetry about its own $u_2 = 0$. Figure 4 depicts the sinusoidal variations of all velocity components across the crest length (L_y) direction, for the same case of $\theta = 45°$, $d/L = 0{\cdot}1$ at time $t/T = 0$.

The vertical water-particle velocities, which hold the suspended materials once they are entrained, should receive further attention. Although both w_1 and w_2 given by (30) and (41) have been shown to imply linear profiles at certain time stages within a wave cycle, as demonstrated in figure 3, their dimensional values are in fact small compared with those of u_1 and u_2, because the boundary-layer approximation is used throughout. This is also because different variable transformations have been used as in (14). Thus the curves of w_1 and w_2 presented in figure 4, because of the non-dimensionalization, are only apparently of the same order as the u and v velocities.

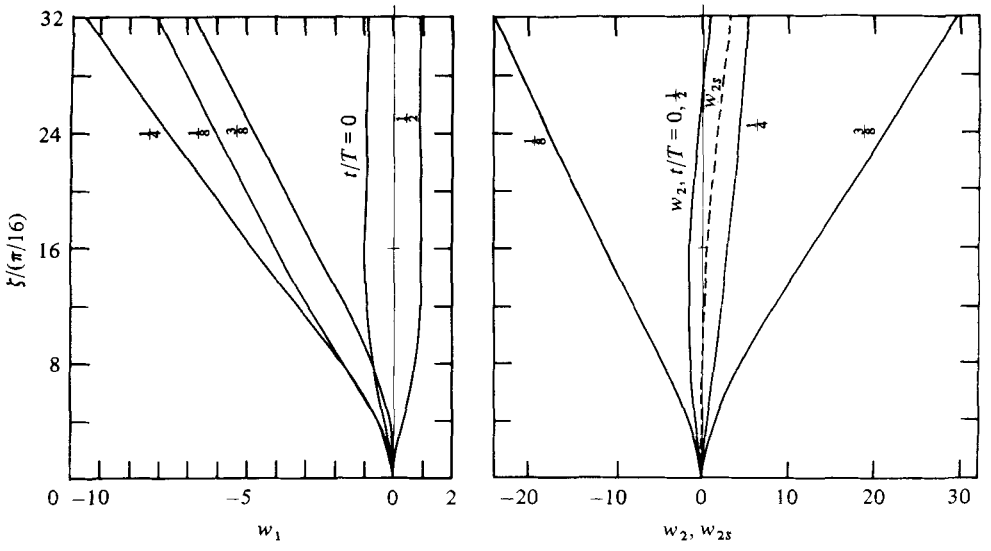

FIGURE 3. Profiles of second-order Eulerian water-particle velocities w_1, w_2 and w_{2s} through the bottom boundary layer at various time steps. $\theta = 45°$, $d/L = 0{\cdot}1$, $y/L_y = 0$ and 1.

4. First approximation to mass transport

The Lagrangian mean velocity for a single water-particle with continuous path is defined as the time-averaged value over one complete wave cycle. This is the convective derivative of position when moving with the particle, or

$$\mathbf{U}_L = d\mathbf{x}/dt = \mathbf{u}(x, y, z, t). \tag{44}$$

Here, $\mathbf{u}(x, y, z, t)$ is the Eulerian velocity vector at the position (x, y, z) at the time $t = (t_0 + \Delta t)$ after some small displacements (ξ_1, ξ_2, ξ_3) from its initial position (x_0, y_0, z_0) at $t = t_0$. The relationship between the Lagrangian and Eulerian velocity, in vector form, is given as

$$\mathbf{U}_L(x_0, y_0, z_0, t) = \mathbf{u}(x_0 + \xi_1, y_0 + \xi_2, z_0 + \xi_3, t). \tag{45}$$

In the three-dimensional case, a function $\hat{f}$ with some small displacements related to its initial position (x_0, y_0, z_0) may be expanded by the Taylor series, yielding (omitting the caret for f)

$$f(x_0 + \xi_1, y_0 + \xi_2, z_0 + \xi_3) = f(x_0, y_0, z_0) + (\xi_1 f_x + \xi_2 f_y + \xi_3 f_z)|_{(x_0, y_0, z_0)} + \frac{1}{2!}(\xi_1^2 f_{xx} + \xi_2^2 f_{yy} + \xi_3^2 f_{zz} + 2\xi_1\xi_2 f_{xy} + 2\xi_2\xi_3 f_{yz} + 2\xi_3\xi_1 f_{zx})|_{(x_0, y_0, z_0)} + \cdots. \tag{46}$$

Upon letting $\mathbf{u} = f$ into (46), and introducing the perturbed series

$$\xi_i = \epsilon\xi_{i1} + \epsilon^2\xi_{i2} + \tfrac{1}{2}\epsilon^3\xi_{i3} + O(\epsilon^4), \quad \text{with} \quad i = 1, 2, 3 \quad \text{for the } x, y \text{ and } z \text{ directions respectively,} \tag{47}$$

$$\hat{u} = \epsilon\hat{u}_1 + \epsilon^2\hat{u}_2 + \tfrac{1}{2}\epsilon^3\hat{u}_3 + O(\epsilon^4), \quad \text{same for } \hat{v} \text{ and } \hat{w}, \tag{48}$$

$$\hat{U}_L = \epsilon\hat{U}_{L1} + \epsilon^2\hat{U}_{L2} + \tfrac{1}{2}\epsilon^3\hat{U}_{L3} + O(\epsilon^4), \quad \text{and so on,} \tag{49}$$

equation (45) yields the necessary equations for deriving the Lagrangian velocity field, in the order of parameter ϵ. The dimensional transforms given by (14) hold valid for (47)–(49).

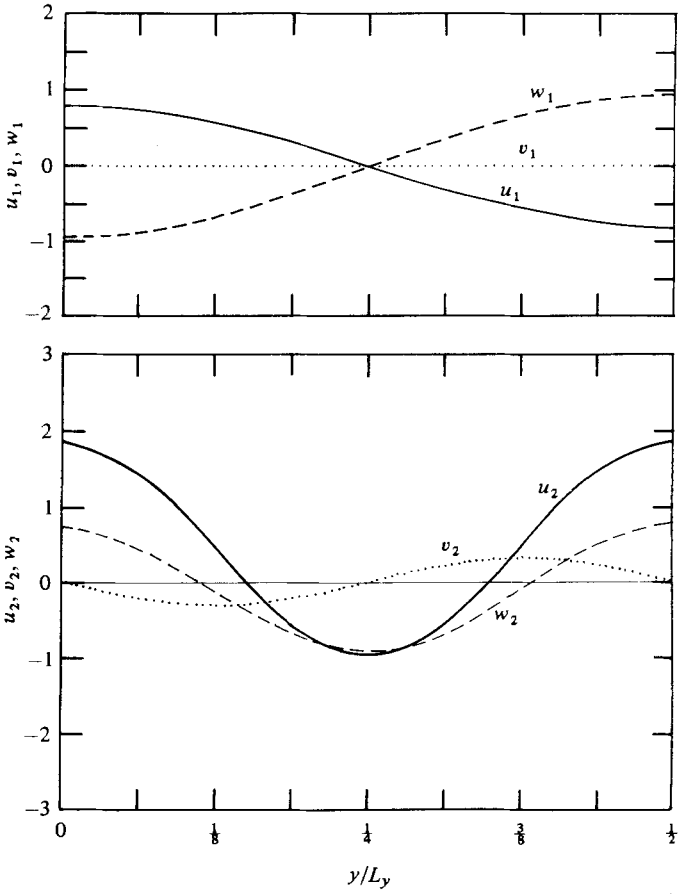

FIGURE 4. Variations of first- and second-order Eulerian water-particle valocites for just beyond the boundary layer as functions of distances from the reflecting wall. $\theta = 45°$, $d/L = 0{\cdot}1$, $t/T = 0$.

Hence for the *first order in* ϵ, the relationships between the Lagrangian and Eulerian velocity as well as the particle displacement are given in dimensionless form as

$$U_{L1} = \omega_0 \frac{d\xi_{11}}{dt} = u_1, \tag{50}$$

$$V_{L1} = \omega_0 \frac{d\xi_{21}}{dt} = v_1, \tag{51}$$

$$W_{L1} = \omega_0 \frac{d\xi_{31}}{dt} = w_1; \tag{52}$$

and, for the *second order in* ϵ, they are

$$U_{L2} = \omega_0 \frac{d\xi_{12}}{dt} = u_2 + (\xi_{11} u_{1x} + \xi_{21} u_{1y} + \xi_{31} u_{1z}), \tag{53}$$

$$V_{L2} = \omega_0 \frac{d\xi_{22}}{dt} = v_2 + (\xi_{11} v_{1x} + \xi_{21} v_{1y} + \xi_{31} v_{1z}), \tag{54}$$

$$W_{L2} = \omega_0 \frac{d\xi_{32}}{dt} = w_2 + (\xi_{11} w_{1x} + \xi_{21} w_{1y} + \xi_{31} w_{1z}). \tag{55}$$

The first-order particle displacements (ξ_{11}, ξ_{21}, ξ_{31}) in the x, y and z directions respectively, can be obtained by integration with respect to time from (50)–(52). The second-order displacements (ξ_{12}, ξ_{22}, ξ_{32}) obtained from (53)–(55) should be used in calculating the second approximation of mass-transport velocity.

To the *third order in* ϵ, more terms are involved in these relationships,

$$U_{L3} = u_3 + 2(\xi_{12}u_{1x} + \xi_{22}u_{1y} + \xi_{32}u_{1z} + \xi_{11}u_{2x} + \xi_{21}u_{2y} + \xi_{31}u_{2z}) + (\xi_{11}^2 u_{1xx} + \xi_{21}^2 u_{1yy} + \xi_{31}^2 u_{1zz}) + 2(\xi_{11}\xi_{21}u_{1xy} + \xi_{21}\xi_{31}u_{1yz} + \xi_{31}\xi_{11}u_{1zx}), \quad (56)$$

$$V_{L3} = v_3 + 2(\xi_{12}v_{1x} + \xi_{22}v_{1y} + \xi_{32}v_{1z} + \xi_{11}v_{2x} + \xi_{21}v_{2y} + \xi_{31}v_{2z}) + (\xi_{11}^2 v_{1xx} + \xi_{21}^2 v_{1yy} + \xi_{31}^2 v_{1zz}) + 2(\xi_{11}\xi_{21}v_{1xy} + \xi_{21}\xi_{31}v_{1yz} + \xi_{31}\xi_{11}v_{1zx}). \quad (57)$$

Equations (56) and (57) allow the second approximation of mass transport to proceed. The limiting expression of U_{L3} from (56) agrees with that of Isaacson (1976), for the two-dimensional case.

It is necessary now to define the mass transport velocity U_M, which may be expressed in the form of dimensionless quantities,

$$U_M = \epsilon U_{M1} + \epsilon^2 U_{M2} + \tfrac{1}{2}\epsilon^3 U_{M3} + O(\epsilon^4), \quad (58)$$

with the same for V_M and W_M. There is no first-order motion, because the time averages of any periodic function over a complete wave cycle would vanish, or $U_{M1} = 0$. Therefore, the first approximation to the mass transport U_{M2} is calculated from the time average of (53) over the whole period of 2π, and also for V_{M2} from (54) and W_{M2} from (55). The calculation of each time step is included in appendix A.

Finally, in dimensionless form, the mass-transport velocity components, U_{M2}, V_{M2} and W_{M2}, within the laminar bottom boundary layer in the short-crested waves, are given as

$$U_{M2} = \frac{m\omega_0}{8\sinh^2 d}\{[5 + 3e^{-2\zeta} - 8e^{-\zeta}\cos\zeta] + [(4m^2+1) + (2m^2+1)e^{-2\zeta} - 8m^2 e^{-\zeta}\cos\zeta]\cos 2ny\}, \quad (59)$$

$$V_{M2} = \frac{n\omega_0}{8\sinh^2 d}[-(2n^2+1) + (2n^2+1)e^{-2\zeta} + 8n^2 e^{-\zeta}\sin\zeta]\sin 2ny, \quad (60)$$

$$W_{M2} = \frac{(2\omega_0)^{\frac{1}{2}}}{8\sinh^2 d}\{n^4[8\sqrt{2}\,e^{-\zeta}\sin(\zeta + \tfrac{1}{4}\pi) + 2e^{-2\zeta} + 4\zeta - 10] + n^2[e^{-2\zeta} + 2\zeta - 1]\}\cos 2ny. \quad (61)$$

Both U_{M2} and V_{M2} are identical to those derived by Mei *et al.* (1972) using the Lagrangian form and linear superposition of two first-order velocity potentials. The above approach (with Eulerian description and the short-crested wave theory to the second order directly) has produced a similar result. This is because the present boundary-layer approach is a first approximation. Also, the time-averaged values of u_2 and v_2 in the right-hand sides of (53) and (54) retain only those time-dependent terms originating from the interaction of the first-order velocities. This similarity is therefore to be expected.

The expression for U_{M2} of (59) can be reduced readily to the horizontal mass transport in dimensional form for a progressive wave as derived by Longuet-Higgins (1953). However, that derived by Mei *et al.* (1972) cannot be so reduced. The multiplying factor in the final expression they derived (i.e. $m_1 ga^2/k\sinh^2 kd$, in the present notation)

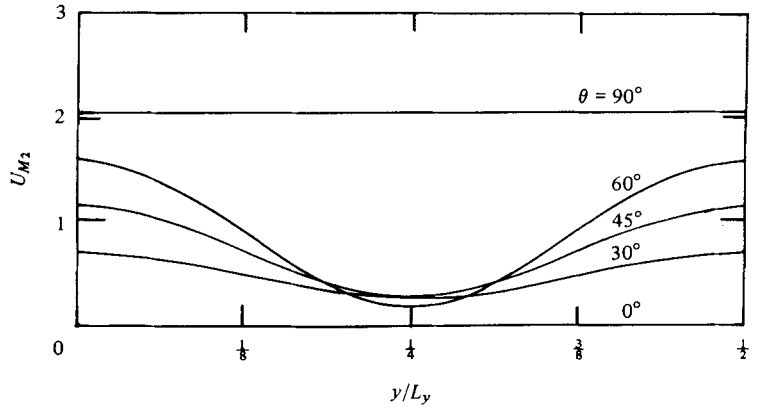

FIGURE 5. Variations of mass transport velocity U_{M2} for just beyond the bottom layer as functions of specific distance from the reflecting wall and the angles of incidence. $d/L = 0{\cdot}1$.

appears incorrect, but even when manipulated correctly (see appendix B) it still results in a mass transport velocity four times too great. This was noted by these authors as 'that in the present case the amplitude of the limiting progressive wave is twice that of' the usual progressive wave (Mei *et al.* 1972, p. 54). This interpretation was repeated in a subsequent publication (Carter, Liu & Mei 1973, p. 173).

As mentioned previously, it is across the plane normal to the direction of propagation that the wave profile, water-particle orbits, velocities and accelerations change significantly. For the dimensionless value of the mass-transport velocity as given by equation (59), the numerical value for U_{M2} as $\zeta \to \infty$ is shown in figure 5 for distances across the crest-length (y/L_y) and the angle of incidence (θ), for the case of $d/L = 0{\cdot}1$. It is clear that U_{M2} is unidirectional with one sign throughout.

The maximum mass transport velocities for various locations are produced in figures 6–8, as functions of the relative vertical distance ζ and θ. It is worth noting that both V_{M2} and W_{M2} show the flow reversal near the bottom for incident angles less than 45°.

5. Experimental data

To observe water-particle motions close to the bed, polystyrene beads between 1 and 1·5 mm diameter and specific gravity 1·03 were carefully placed on the perspex zone of the bed in a wave basin. The wave basin had a unique T-shaped tunnel, of $1{\cdot}8 \times 2{\cdot}1$ m cross-section, constructed beneath it (Hsu 1977). The tracers used were about one-third of the boundary-layer thickness, which would have made comparison with theory difficult. But as a first attempt at verification of horizontal velocities and mass transport at the bed the procedure was believed to be both novel and realistic. The introduction of a slight negative buoyancy (with specific gravity 1·03) helped to retain the beads in the bottom layer during motion.

A set of experimental data was obtained from a test case of short-crested waves, with $\theta = 45°$, $d/L = 0{\cdot}213$ and $H/L = 0{\cdot}060$ (from $T = 0{\cdot}975$ s, $d = 290$ mm, incident wave height $H = 82$ mm, and the resulting short-crested wave height $H_{sc} = 165$ mm). The orbital motions as illustrated in figure 9 show the recorded positions of beads at

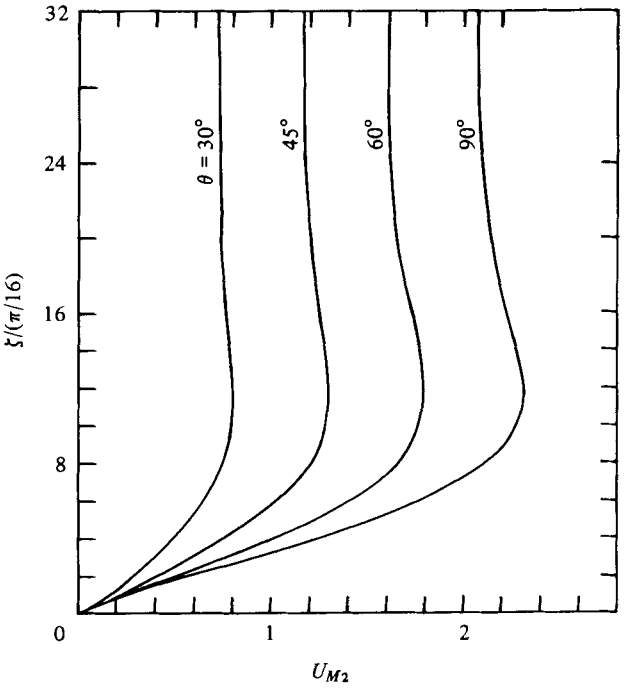

FIGURE 6. Mass transport velocity profiles of U_{M_2} through the bottom boundary layer for various angles of incidence. The curve for $\theta = 90°$ (progressive wave) agrees with Longuet-Higgins (1953). $d/L = 0{\cdot}1$, $y/L_y = 0$, $\frac{1}{2}$ and 1.

every $\frac{1}{12}$ s interval over one complete wave cycle (dots on the curve). The square symbols indicate the locations after each wave cycle. The orbits are seen to change in character with distance (y/L_y) from the reflecting wall.

A comparison, in fact, was made with mass transport in progressive waves in order to assess a scale factor which could be applied to the measurements in short-crested waves, as the former has been well established.

Given a test case, a progressive wave of period 1·0 s and 80 mm height, propagated in 303 mm of water depth with water temperature close to the bed at 20 °C and a bottom-layer thickness of 3·545 mm was calculated from $\delta = 2(\pi\nu T)^{\frac{1}{2}}$. For a polystyrene bead with 1·5 mm diameter, its centre-line was located at $0{\cdot}212\delta$ from the bed (i.e. the ratio of 0·75/3·545), or in other words, at a reading of 6·8 on the vertical scale (i.e. $0{\cdot}212 \times 32$, with a scale of 32 representing the condition at the outer edge of the bottom layer).

The theoretical profile of the mass transport velocity through the bottom layer is shown in figure 10(*a*), as well as the size of the tracer bead and its centre-line. The theoretical velocity at the centre-line is about 12·6 mm s^{-1}. The measured mass transport velocities over 8 continuous wave cycles were 5·0, 6·5, 8·0, 6·5, 6·5, 5·5, 7·0 and 7·5 mm s^{-1} consecutively, with an average of 6·56 mm s^{-1}. These are also illustrated in the same figure. Thus the scale factor was 0·52 (being the ratio of 6·56/12·6).

It is seen that the measured mass transport in this case of a progressive wave corresponds to a vertical reading of about 3 or 4, say, in figure 10(*a*), at about a quarter of its diameter from the bed.

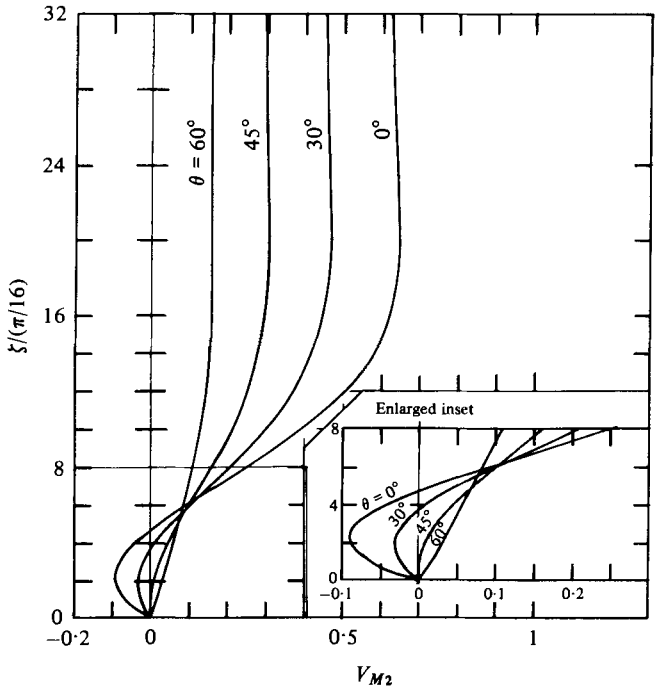

FIGURE 7. Mass transport velocity profiles of V_{M2} through the bottom boundary layer for various angles of incidence. The curve for $\theta = 0°$ (standing wave) agrees with Longuet-Higgins (1953). $d/L = 0{\cdot}1$, $y/L_y = \frac{3}{8}$ and $\frac{7}{8}$.

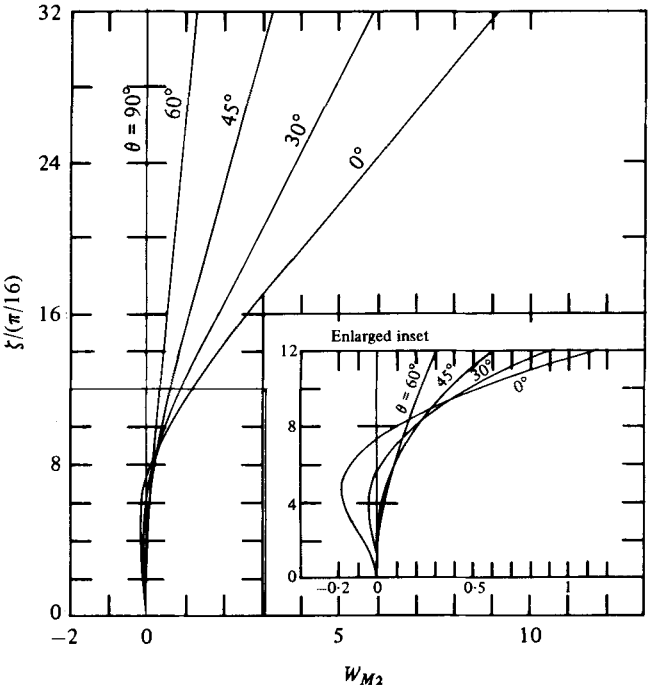

FIGURE 8. Mass transport velocity profiles of W_{M2} through the bottom boundary layer for various angles of incidence. $d/L = 0{\cdot}1$, $y/L_y = \frac{1}{4}$ and $\frac{3}{4}$.

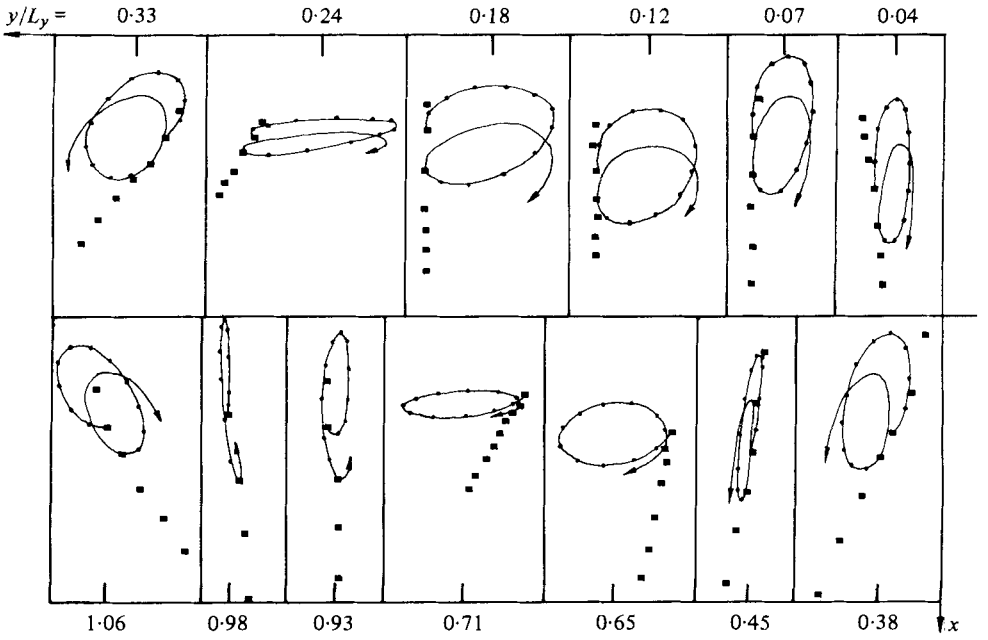

FIGURE 9. Orbital paths of beads recorded at specified distances from the reflecting wall. Circular dots indicating position at $\frac{1}{12}$ time interval of the wave period, squared points for position after each wave cycle. $\theta = 45°$, $T = 0{\cdot}975$ s, $d/L = 0{\cdot}312$, $\epsilon = 0{\cdot}364$.

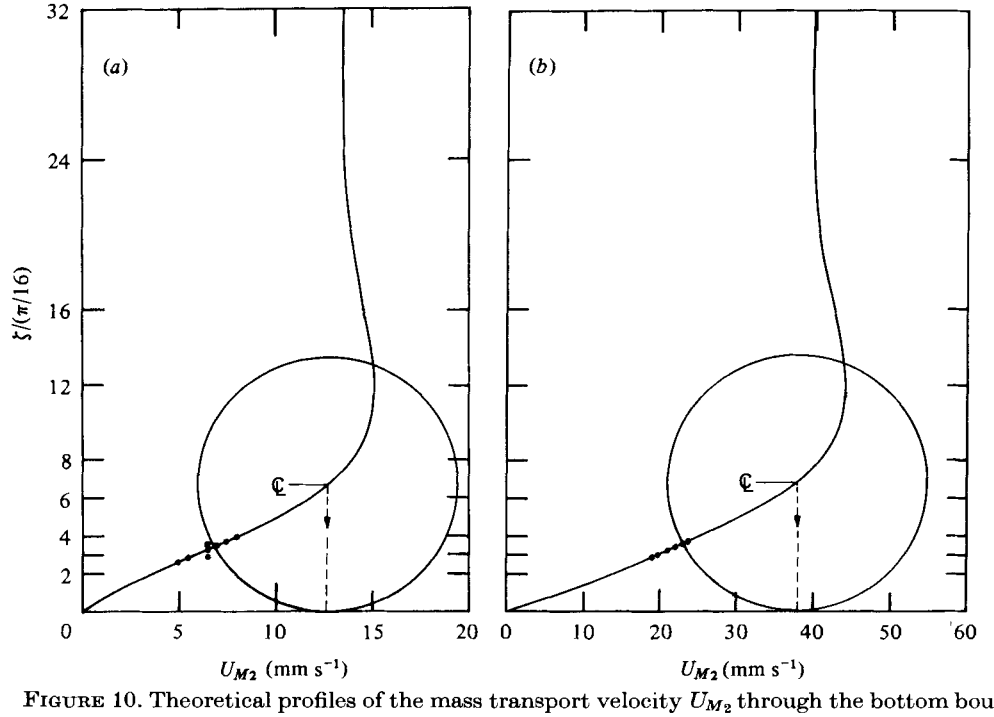

FIGURE 10. Theoretical profiles of the mass transport velocity U_{M_2} through the bottom boundary layer, showing also the measured values plus the size of the tracer bead. (*a*) For a case of progressive waves, $T = 1{\cdot}0$ s, $H = 80$ mm, $d = 303$ mm. (*b*) For a case of short-crested waves, $\theta = 45°$, $T = 0{\cdot}975$ s, $H_{sc} = 165$ mm, $d = 290$ mm, at $y/L_y = 0{\cdot}98$ from the wall.

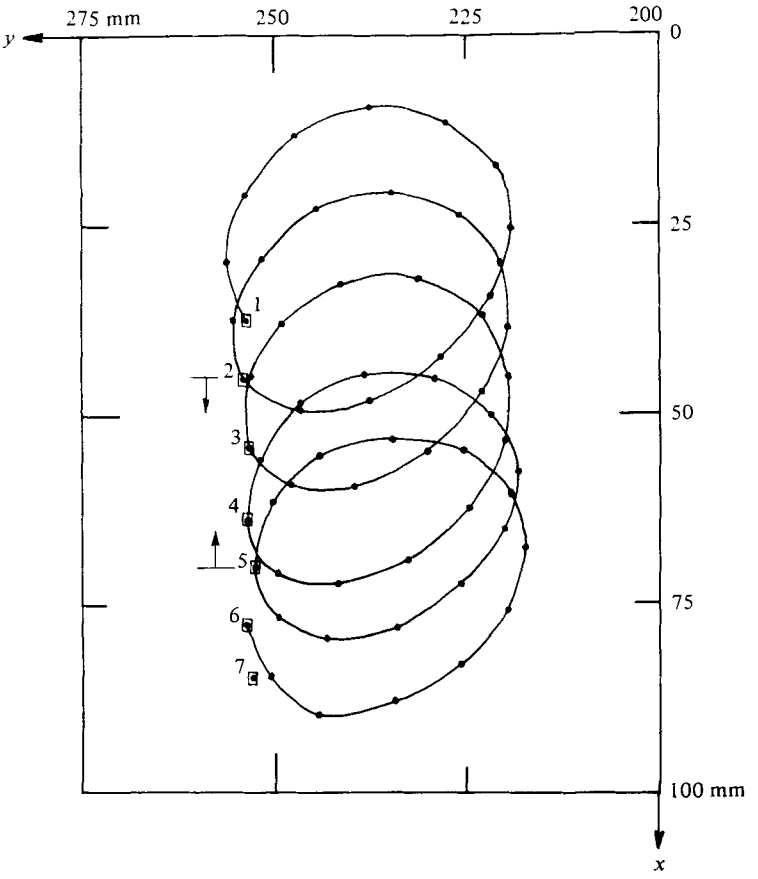

FIGURE 11. Series of six orbits recorded at $y/L_y = 0{\cdot}12$ from the wall, for the same case of short-crested waves as in figure 9.

For the same test case of short-crested waves at $y/L_y = 0{\cdot}98$ as in figure 9, the thickness of the wave boundary layer was 3·50 mm. Hence the centre of the tracer bead was about $0{\cdot}214\delta$ from the bed (for a bead diameter of 1·5 mm) and was thus located at a reading of 6·86 on the vertical scale, as shown in figure 10(*b*). The recorded values of mass transport U_{M2} over six continuous orbits were 22·5, 23·0, 19·0, 23·5, 22·0 and 19·5 mm s^{-1} respectively, with an average of 21·58 mm s^{-1}. These measured mass transport velocities also correspond to the vertical scale between 3 and 4 as indicated in figure 10(*b*), similar to that of the progressive wave case in figure 10(*a*). The scale factor from this was thus at 0·56 (being the ratio of 21·58/38·5, in which the value 38·5 was the expected U_{M2} at the centre-line). This scale factor agrees very well with that obtained from the progressive wave case above (being at 0·52).

The orbital motions as illustrated in figure 11 show the recorded positions of a bead at every $\frac{1}{12}$ s interval over 6 complete wave orbits, for the case of $y/L_y = 0{\cdot}12$ depicted in figure 9. The horizontal tracer velocities U_L and V_L, derived from the 3 continuous wave cycles (i.e. from the squared points 2–5 inclusive), were used and compared (figure 12) with theory from (49).

The experimental data in figure 12 follow the theoretical curves of u_4 and v_4 within

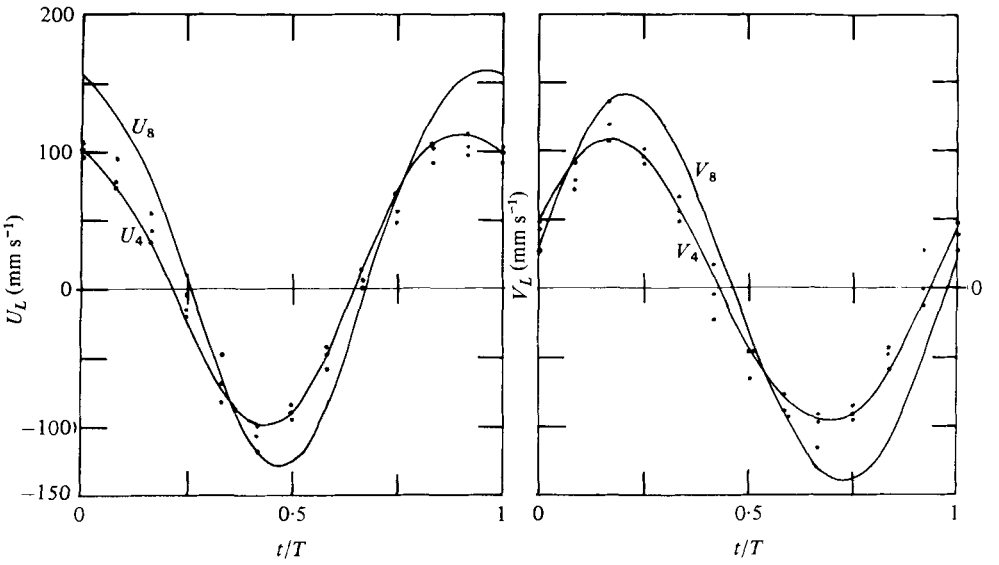

FIGURE 12. A comparison of measured Lagrangian horizontal velocities U_L and V_L close to the bed with the theoretical curves, as function of time, for a case of short-crested waves as in figure 9. The curves of (u_4, v_4, u_8, v_8) being the theoretical water-particle velocities at the reading of 4 and 8 respectively on the vertical scale in figure 10(*b*).

acceptable limits (here u_4 and v_4 refer to the theoretical particle velocities at the reading of 4 on the vertical scale in figure 10*b*). It is obvious from figures 10(*b*) and 12 that the measured mass transport U_{M2} and the Lagrangian tracer velocities U_L and V_L were all referred to the same level of reference from the bed, i.e. a reading of about 4 on the vertical scale in these figures. This agreement was sufficient to prove that the beads were moved consistently within the boundary layer.

6. Two-dimensional limiting cases

As the general three-dimensional equations are rather complicated for visualizing the action directly, it seems appropriate to present the complete equations of the two-dimensional cases for the limiting angles of approach. These include the expressions for the Eulerian water-particle velocities and mass transport, all within the laminar boundary layer at the bed.

For the present short-crested wave theory, equations for the usual progressive wave can be obtained when $m = 1$ and $n = 0$, and for the normal standing wave when $m = 0$ and $n = 1$. All coefficients of Q are then simplified. The results in dimensionless form are as follows.

For *progressive waves*, $Q_1' = 3\omega_0/4\sinh^4 d$, $Q_2' = Q_3' = \omega_0/4\sinh^2 d$, thus

$$u_1 = [\omega_0/\sinh(d)][\cos(x-t) - e^{-\zeta}\cos(x-t+\zeta)], \tag{62}$$

$$w_1 = [-\omega_0^{\frac{1}{2}}/\sinh(d)][\sqrt{2}\,\zeta\sin(x-t) - \sin(x-t+\tfrac{1}{4}\pi) + e^{-\zeta}\sin(x-t+\zeta+\tfrac{1}{4}\pi)], \tag{63}$$

$$\begin{aligned} u_2 = {} & Q_1'\cos(2x-2t) + 2Q_2'\,e^{-\zeta}\cos(2x-2t+\zeta) - 2\sqrt{2}\,Q_2'\zeta e^{-\zeta}\cos(2x-2t+\zeta-\tfrac{1}{4}\pi) \\ & - (Q_1'+2Q_2')\,e^{-\sqrt{(2)}\zeta}\cos(2x-2t+\sqrt{2}\,\zeta) \\ & + Q_2'[2e^{-\zeta}(\sin\zeta - 2\cos\zeta) - 2\sqrt{2}\,\zeta e^{-\zeta}\cos(\zeta-\tfrac{1}{4}\pi) + e^{-2\zeta} + 3], \end{aligned} \tag{64}$$

$$w_2 = (2/\omega_0)^{\frac{1}{2}}[2Q_1'\zeta\sin 2(x-t) - (Q_1'+2Q_2')\sin(2x-2t-\tfrac{1}{4}\pi) + 4Q_2'\zeta e^{-\zeta}\sin(2x-2t+\zeta) + (Q_1'+2Q_2')e^{-\sqrt{(2)}\zeta}\sin(2x-2t+\sqrt{2}\,\zeta+\tfrac{1}{4}\pi)], \quad (65)$$

and

$$U_{M2} = [\omega_0/4\sinh^2 d](5+3e^{-2\zeta}-8e^{-\zeta}\cos\zeta), \quad (66)$$

$$V_{M2} = W_{M2} = 0. \quad (67)$$

For *standing waves*, $Q_4' = 3Q_5'/\sinh^2 d = 3\omega_0/8\sinh^4 d$, thus

$$v_1 = [\omega_0/\sinh(d)][\sin t - e^{-\zeta}\sin(t-\zeta)]\sin y, \quad (68)$$

$$w_1 = [\omega_0^{\frac{1}{2}}/\sinh(d)][\sqrt{2}\,\zeta\sin t - \sin(t-\tfrac{1}{4}\pi) + e^{-\zeta}\sin(t-\zeta-\tfrac{1}{4}\pi)]\cos y, \quad (69)$$

$$v_2 = [Q_4'\sin 2t + 2Q_5'e^{-\zeta}\sin(2t-\zeta) - 2\sqrt{2}\,Q_5'\zeta e^{-\zeta}\sin(2t-\zeta+\tfrac{1}{4}\pi) - (Q_4'+2Q_5')e^{-\sqrt{(2)}\zeta}\sin(2t-\sqrt{2}\,\zeta)]\sin 2y + Q_5'[8e^{-\zeta}\sin\zeta + 2e^{-\zeta}\cos\zeta + 2\sqrt{2}\,\zeta e^{-\zeta}\sin(\zeta-\tfrac{1}{4}\pi) + e^{-2\zeta} - 3]\sin 2y, \quad (70)$$

$$w_2 = (2/\omega_0)^{\frac{1}{2}}[-2Q_4'\zeta\sin 2t + (Q_4'+2Q_5')\sin(2t-\tfrac{1}{4}\pi) - 4Q_5'\zeta e^{-\zeta}\sin(2t-\zeta) - (Q_4'+2Q_5')e^{-\sqrt{(2)}\zeta}\sin(2t-\sqrt{2}\,\zeta-\tfrac{1}{4}\pi)]\cos 2y + (2/\omega_0)^{\frac{1}{2}}[8\sqrt{2}\,e^{-\zeta}\sin(\zeta+\tfrac{1}{4}\pi) + 4\zeta e^{-\zeta}\sin\zeta + 4e^{-\zeta}\cos\zeta + e^{-2\zeta} + 6\zeta - 13]Q_5'\cos 2y, \quad (71)$$

and

$$V_{M2} = [\omega_0/8\sinh^2 d](-3+3e^{-2\zeta}+8e^{-\zeta}\sin\zeta)\sin 2y, \quad (72)$$

$$W_{M2} = [(2\omega_0)^{\frac{1}{2}}/8\sinh^2 d][-11+6\zeta+3e^{-2\zeta}+8\sqrt{2}\,e^{-\zeta}\sin(\zeta+\tfrac{1}{4}\pi)]\cos 2y. \quad (73)$$

The dimensional equations for (u_1, v_1, w_1) and (u_2, u_2) agree with that derived by Noda (1970). However, w_2 had not been attempted for either limiting case.

The dimensional expressions for U_{M2}, V_{M2} and W_{M2} can readily be obtained from (66), (67), (72) and (73) by variable transformations as in (14). The velocity profiles of U_M and V_M from (66) and (72) agree with those of Longuet-Higgins (1953, p. 567, equation (253)). Thus, for just beyond the bottom boundary layer, at $\zeta = 2\pi$ (i.e. for $\zeta \to \infty$ theoretically), these equations become,

for progressive waves,

$$U_{M2} = \frac{5\,k\sigma a^2}{4\sinh^2 kd}, \quad (74)$$

$$V_{M2} = W_{M2} = 0, \quad (75)$$

and, for standing waves,

$$V_{M2} = -\frac{3\,k\sigma a^2}{8\sinh^2 kd}\sin 2ky, \quad (76)$$

$$W_{M2} = \frac{37{\cdot}7583}{8}[k(\nu/\sigma)^{\frac{1}{2}}]\frac{k\sigma a^2}{\sinh^2 kd}\cos 2ky, \quad (77)$$

in which the notation a denotes the amplitude of progressive and standing waves respectively. Again, the dimensional limiting values of U_{M2} and V_{M2} from (74) and (76) agree with the well-known equations given by Longuet-Higgins (1953, equations (255) and (262)).

The physical significance of equations (74)–(77) is demonstrated by the following calculation. Given a 10 s wave train in 5 m water depth, with average water temperature at 25 °C, then $L = 67{\cdot}64$ m, $k = 0{\cdot}093$, $\sigma = 0{\cdot}628$ and $\nu = 0{\cdot}93\,\text{mm}^2\,\text{s}^{-1}$. Therefore

for a progressive wave, $U_{M2}/(k\sigma a^2/\sinh^2 kd) = 1{\cdot}250$ from (74) and, for the standing wave, $V_{M2}/(k\sigma a^2/\sinh^2 kd) = 0{\cdot}375$ from (76). Thus, the ratio $U_{M2}/V_{M2} = 3{\cdot}33$ for the same wave amplitude a. Within the standing wave itself, W_{M2} at the anti-node is about 1·424 (or 0·534/0·375) times as great as the V_{M2} value at nodal point, as derived from (77) and (76). This could well explain the reason for the strong suspension at the anti-nodal position in standing waves. It might also constitute the vertical 'jet-like' motions beneath the anti-nodal points, as reported by Mei *et al.* (1972) and Dore (1976).

The senior author is grateful for the helpful suggestion from Dr B. D. Dore of the University of Reading, and to the referees, for their constructive comments on secular terms which have led to a number of improvements of this work.

Appendix A

The derivation of mass transport velocities by the time-averaging process from equations (53)–(55) is as follows.

It is more convenient to process all the time-averaged steps by means of complex variables. Thus the time-average of two functions of A and B may be expressed as

$$\overline{AB} = \frac{\sigma}{2\pi}\int_t^{t+(2\pi/\sigma)} (AB)\,dt' = \tfrac{1}{2}\,\mathrm{Re}\,[A_0 B_0^*] = \tfrac{1}{2}\,\mathrm{Re}\,[A_0^* B_0], \tag{78}$$

in which $A = A_0 \exp(i\sigma t)$, $B = B_0 \exp(i\sigma t)$; where Re indicates the real part and $*$ the conjugated part of a complex variable. Taking the mass transport in the x direction for example yields, from (53),

$$U_{M2} = \bar{u}_2 + \frac{1}{\omega_0}\left[\overline{u_{1x}\cdot\int_0^t u_1\,dt'} + \overline{u_{1y}\cdot\int_0^t v_1\,dt'} + \overline{u_{1z}\cdot\int_0^t w_1\,dt'}\right], \tag{79}$$

where the overbar denotes the time average over one wave period, similarly,

$$V_{M2} = \bar{v}_2 + \frac{1}{\omega_0}\left[\overline{v_{1x}\cdot\int_0^t u_1\,dt'} + \overline{v_{1y}\cdot\int_0^t v_1\,dt'} + \overline{v_{1z}\cdot\int_0^t w_1\,dt'}\right], \tag{80}$$

$$W_{M2} = \bar{w}_2 + \frac{1}{\omega_0}\left[\overline{w_{1x}\cdot\int_0^t u_1\,dt'} + \overline{w_{1y}\cdot\int_0^t v_1\,dt'} + \overline{w_{1z}\cdot\int_0^t w_1\,dt'}\right]. \tag{81}$$

By inserting the first-order Eulerian velocity components, u_1, v_1 and w_1 from (28)–(30), and the second-order solutions of u_2, v_2 and w_2 from (37), (38) and (41), into equations (79)–(81), the results of each averaged step can be obtained:

$$\bar{u}_2 = \frac{m\omega_0}{4\sinh^2 d}[2e^{-\zeta}(\sin\zeta - 2\cos\zeta) - 2\zeta e^{-\zeta}(\sin\zeta + \cos\zeta) + e^{-2\zeta} + 3]\cos^2 ny, \tag{82}$$

$$\overline{u_{1x}\cdot\int_0^t u_1\,dt'} = \frac{m^3\omega_0^2}{2\sinh^2 d}[1 - 2e^{-\zeta}\cos\zeta + e^{-2\zeta}]\cos^2 ny, \tag{83}$$

$$\overline{u_{1y}\cdot\int_0^t v_1\,dt'} = \frac{mn^2\omega_0^2}{2\sinh^2 d}[1 - 2e^{-\zeta}\cos\zeta + e^{-2\zeta}]\sin^2 ny, \tag{84}$$

$$\overline{u_{1z}\cdot\int_0^t w_1\,dt'} = \frac{m\omega_0^2}{2\sinh^2 d}[\zeta e^{-\zeta}(\sin\zeta + \cos\zeta) - e^{-\zeta}\sin\zeta]\cos^2 ny, \tag{85}$$

$$\bar{v}_2 = \frac{n\omega_0}{8\sinh^2 d}[2n^2(4e^{-\zeta}\sin\zeta + e^{-2\zeta} - 1) + 2e^{-\zeta}\cos\zeta + 2\zeta e^{-\zeta}(\sin\zeta - \cos\zeta) - e^{-2\zeta} - 1]\sin 2ny, \quad (86)$$

$$\overline{v_{1x}\cdot\int_0^t u_1\,dt'} = \overline{v_{1y}\cdot\int_0^t v_1\,dt'} = 0, \quad (87)$$

$$\overline{v_{1z}\cdot\int_0^t w_1\,dt'} = \frac{n\omega_0^2}{4\sinh^2 d}[\zeta e^{-\zeta}(-\sin\zeta + \cos\zeta) - e^{-\zeta}\cos\zeta + e^{-2\zeta}]\sin 2ny, \quad (88)$$

and consequently

$$\bar{w}_2 = \frac{(2\omega_0)^{\frac{1}{2}}n^4}{4\sinh^2 d}[4\sqrt{2}\,e^{-\zeta}\sin(\zeta + \tfrac{1}{4}\pi) + e^{-2\zeta} + 2\zeta - 5)\cos 2ny + \frac{(2\omega_0)^{\frac{1}{2}}n^2}{4\sinh^2 d}[2\zeta e^{-\zeta}\sin\zeta + 2e^{-\zeta}\cos\zeta - \tfrac{1}{2}e^{-2\zeta} + \zeta - \tfrac{3}{2}]\cos 2ny, \quad (89)$$

$$\overline{w_{1x}\cdot\int_0^t u_1\,dt'} = \frac{(2\omega_0)^{\frac{1}{2}}m^2\omega_0}{4\sinh^2 d}[2\zeta e^{-\zeta}\sin\zeta + 2e^{-\zeta}\cos\zeta - e^{-2\zeta} - 1]\cos^2 ny, \quad (90)$$

$$\overline{w_{1y}\cdot\int_0^t v_1\,dt'} = \frac{(2\omega_0)^{\frac{1}{2}}n^2\omega_0}{4\sinh^2 d}[2\zeta e^{-\zeta}\sin\zeta + 2e^{-\zeta}\cos\zeta - e^{-2\zeta} - 1]\sin^2 ny, \quad (91)$$

$$\overline{w_{1z}\cdot\int_0^t w_1\,dt'} = -\frac{(2\omega_0)^{\frac{1}{2}}\omega_0}{4\sinh^2 d}[2\zeta e^{-\zeta}\sin\zeta + 2e^{-\zeta}\cos\zeta - e^{-2\zeta} - 1]\cos^2 ny. \quad (92)$$

Thus, the final expressions for U_{M2}, V_{M2} and W_{M2} of (79)–(81) can be readily derived. The results are given as equations (59)–(61) in the text.

Appendix B

The final expression of the mass transport velocity U_{M2} in a short-crested wave as derived by Mei *et al.* (1972) and subsequently repeated by Carter *et al.* (1973), in dimensional form was given as

$$U_{M2} = \frac{m_1 ga^2}{k\sinh^2 kd}\{[8m_1^2\cos 2n_1 y + 8k^2]e^{-\zeta}\cos\zeta - [(3m_1^2 - n_1^2)\cos 2n_1 y + 3k^2]e^{-2\zeta} - [(5m_1^2 + n_1^2)\cos 2n_1 y + 5k^2]\}, \quad (93)$$

using the present notation, in which $m_1^2 + n_1^2 = k^2$. Thus, just beyond the bottom layer, at $\zeta \to \infty$, and for the limiting progressive wave with $m_1 = k$ and $n_1 = 0$, equation (93) becomes

$$U_{M2} = -10gk^2a^2/\sinh^2 kd. \quad (94)$$

This does not agree with that of Longuet-Higgins (1953) nor (74) in the text. After following through the calculation procedure it was found that the correct expression should read

$$U_{M2} = \frac{m_1 ga^2}{k\sigma\sinh^2 kd}\{\text{the same expression in the bracket as (93)}\}, \quad (95)$$

so that

$$U_{M2} = -5k\sigma a^2/\sinh^2 kd, \quad (96)$$

which is also four times greater than the value given in (74).

REFERENCES

CARTER, T. G., LIU, P. L.-F. & MEI, C. C. 1973 Mass transport by waves and offshore sand bedforms. *J. Waterways, Harbours & Coastal Engng Div., A.S.C.E.* **99** (WW2), 165–184.

DORE, B. D. 1973 On steady particle motion in circular gravity waves. *Acta Mech.* **17**, 227–245.

DORE, B. D. 1974 The mass transport velocity due to interacting wave trains. *Meccanica*, **9**, 172–178.

DORE, B. D. 1976 Double boundary layers in standing surface waves. *Pure & Appl. Geophys.* **114**, 629–637.

HSU, J. R. C. 1977 Kinematics of short-crested water waves. *Proc. 6th Austral. Conf. Hydraul. Fluid Mech., Adelaide*, pp. 56–59.

HSU, J. R. C., TSUCHIYA, Y. & SILVESTER, R. 1979 Third-order approximation to short-crested waves. *J. Fluid Mech.* **90**, 179–196.

HUNT, J. N. & JOHNS, B. 1963 Currents induced by tides and gravity waves. *Tellus*, **15**, 343–351.

ISAACSON, M. DE ST Q. 1976 The second approximation to mass transport in conoidal waves. *J. Fluid Mech.* **78**, 445–457.

IWAGAKI, Y. & TSUCHIYA, Y. 1966 Laminar damping of oscillatory waves due to bottom friction. *Proc. 10th Conf. on Coastal Engng, vol.* II, pp. 149–174.

LIU, A.-K. & DAVIS, S. H. 1977 Viscous attenuation of mean drift in water waves. *J. Fluid Mech.* **81**, 63–84.

LONGUET-HIGGINS, M. S. 1953 Mass transport in water waves. *Phil. Trans. Roy. Soc.* A, **245**, 535–581.

MEI, C. C., LIU, P. L.-F. & CARTER, T. G. 1972 Mass transport in water waves. *M.I.T., Ralph M. Parsons Lab. Rep.* 146.

NODA, H. 1968 A study on mass transport in boundary layers in standing waves. *Proc. 11th Conf. on Coastal Engng, London*, pp. 227–247.

NODA, H. 1970 The basic study on coastal littoral drift. Ph.D. thesis, Kyoto University, Japan. (In Japanese.)

PRANDTL, L. 1904 *Proc. 3rd Intl Math. Cong., Heidelberg*, pp. 484–491. (In German.) Also available in English (Motion of fluids with very little viscosity. *Tech. Memor. Nat. Adv. Comm. Aero., Washington*, no. 452, 1928.)

SCHLICHTING, H. 1968 *Boundary-layer theory*, 6th edn (translated from German by J. Kestin), pp. 411–414. McGraw-Hill.

SILVESTER, R. 1972 Wave reflection at seawalls and breakwaters. *Proc. Inst. Civil Eng.*, vol. 54, pp. 123–131.

SILVESTER, R. 1977 The role of wave reflection in coastal processes. *Proc. Coastal Sediment* 77, *A.S.C.E.*, pp. 639–654.

STUART, J. T. 1963 *Laminar Boundary-Layers* (ed. L. Rosenhead), chap. 7, pp. 382–384. Oxford University Press.

TANAKA, N., IRIE, I. & OZASA, H. 1972 A study on the velocity distribution of mass transport caused by diagonal partial standing waves. *Rep. Port & Harbour Res. Inst., Japan*, **11**, 112–140. (In Japanese.)